Copy 6
RM L53E25

NACA RM L53E25

NACA

# RESEARCH MEMORANDUM

## THE EFFECT OF NACELLE COMBINATIONS AND SIZE ON THE ZERO-LIFT DRAG OF A 45° SWEPTBACK WING AND BODY CONFIGURATION AS DETERMINED BY FREE-FLIGHT TESTS AT MACH NUMBERS BETWEEN 0.8 AND 1.3

By Sherwood Hoffman and William B. Pepper, Jr.

Langley Aeronautical Laboratory
Langley Field, Va.



NATIONAL ADVISORY COMMITTEE
FOR AERONAUTICS

WASHINGTON
June 22, 1953

[redacted]

NATIONAL ADVISORY COMMITTEE FOR AERONAUTICS

RESEARCH MEMORANDUM

# THE EFFECT OF NACELLE COMBINATIONS AND SIZE ON THE ZERO-LIFT DRAG OF A 45° SWEPTBACK WING AND BODY CONFIGURATION AS DETERMINED BY FREE-FLIGHT TESTS AT MACH NUMBERS BETWEEN 0.8 AND 1.3

By Sherwood Hoffman and William B. Pepper, Jr.

## SUMMARY

The effect on zero-lift drag of varying the size and number of symmetrically mounted nacelles on a 45° sweptback wing and body combination has been determined through free-flight tests of rocket-propelled models over a range of Mach numbers from 0.8 to 1.3 and Reynolds numbers from $4 \times 10^6$ to $7 \times 10^6$ based on the wing mean aerodynamic chord. The configurations tested had the following nacelle arrangements on each wing panel: a twin-engine nacelle near the fuselage; a combination of single-engine nacelles, one located at the wing tip and one near the fuselage; a large nacelle at the wing tip; and a large nacelle near the fuselage.

The drag rises of the models were found to be in general agreement with the concepts of the transonic drag-rise rule. For an aircraft similar to the basic configuration used herein and requiring the thrust equivalency of four (present-day) turbojet engines, use of single-engine nacelles combined at the inboard and wing-tip positions on the wing panel or of large engine nacelles at the wing tips would be most desirable from consideration of the drag. Increasing the size of the single-engine nacelle to that of the large nacelle or twin-engine nacelle resulted in an increase in nacelle-plus-interference drag coefficient, especially near Mach number 1.0. The drag-rise Mach number of the basic configuration was reduced from 0.96 to about 0.90 by adding the large or single-engine nacelles to the wing and to about 0.88 by mounting the twin-engine nacelle near the fuselage.

[redacted]

## INTRODUCTION

As part of a general transonic research program of the National Advisory Committee for Aeronautics to investigate the aerodynamic characteristics of promising aircraft configurations, the Langley Pilotless Aircraft Research Division (at its testing station at Wallops Island, Va.) has tested a series of rocket-propelled free-flight models to determine the effect of nacelle location on the zero-lift drag of a high-aspect-ratio, 45° sweptback wing and body combination. In previous papers (refs. 1 to 5), a twin-engine aircraft with single turbojet engine nacelles (about 50 inches in diameter, full scale) was assumed in order to study individual nacelle interference on each wing panel. However, such an aircraft would require about twice the thrust available from the two engines to attain low supersonic speeds. In an attempt to provide drag increments for engine installations meeting the thrust requirements of a supersonic aircraft, tests were made of the wing-body configuration used previously with a large single nacelle which could accommodate a large engine having about twice the thrust available from present-day types of turbojet engines and with two single turbojet engine nacelles located at the wing tip and wing root. The nacelle positions at the wing tip and root were selected because of the favorable interference effects indicated by tests of the single-engine nacelles in reference 2.

The nacelles were made solid by fairing the nose inlet to a point on the premise that the nacelle-plus-interference drag would be about the same for the solid and ducted nacelles at corresponding Mach numbers. This premise was based on previous tests reported in reference 6 of the solid and ducted nacelles at the wing tips. The tests showed that making the nacelle solid in the manner prescribed had a negligible effect on the nacelle-plus-interference drag throughout the test Mach number range.

Flight tests covered a continuous range of Mach numbers varying between 0.8 and 1.30 corresponding to Reynolds numbers of about $4 \times 10^6$ to about $7 \times 10^6$ based on the mean aerodynamic chord of the wing.

## MODELS

The wing-body-fin combination (fig. 1) used for this investigation was the same as that used in references 1 to 6. Coordinates of the fuselage, airfoil section, and nacelles are given in tables I to IV. Nacelle dimensions are given in figure 2 and details of the nacelle locations and the axial distribution of cross-sectional areas of the models are shown in figure 3, where L is the distance from the body nose and A is cross-sectional area. The photographs of the models are presented in figure 4.

[redacted]

The wing had a sweepback angle of 45° along the quarter-chord line, an aspect ratio of 6.0 (based on total wing plan-form area), a taper ratio of 0.6, and an NACA 65A009 airfoil section in the free-stream direction. The leading edge of the wing intersected the fuselage contour at the maximum-diameter station. The fuselage fineness ratio was 10.0 and the ratio of total wing plan-form area to fuselage frontal area was 16.0.

The single-engine nacelle (fig. 2(a)) was a solid body of revolution having a nose plug, an NACA 1-50-250 nose-inlet profile, a cylindrical midsection, and an afterbody with the proportions of form 111 (ref. 1). The fineness ratio of this single-engine solid nacelle was 9.66. The twin-engine nacelle shown in figure 2(b) was formed by placing two single-engine nacelles tangent to each other along the cylindrical portion and fairing between them with straight line elements. The large nacelle, which had a fineness ratio of 8.56 (fig. 2(c)), was formed by scaling up the coordinates of the inlet and afterbody of the single-engine nacelle by a factor of 1.5 and leaving the cylindrical section the same length as was used for the single-engine nacelle.

For convenience, information on the models presented in this paper is tabulated below to indicate the nacelles used and the nacelle positions. The semispan locations are measured between the fuselage and nacelle center lines in percent of the semispan. The chordwise locations are measured along the nacelle center line between the nacelle nose and wing maximum thickness (0.4c) in percent of the mean aerodynamic chord. All the nacelles were symmetrically mounted on the wing.

| Model | Nacelle | Semispan location, percent b/2 | Chordwise location, percent M.A.C. |
|---|---|---|---|
| A | Twin-engine | 19 | 116 |
| B | Large | 20 | 163 |
| C | Large | 94 | 163 |
| D | Single-engine | 18 and 96 | 116 and 116 |
| E (ref. 2) | Single-engine | 18 | 116 |
| F (ref. 2) | Single-engine | 96 | 116 |
| G (ref. 1) | None | -- | --- |

[redacted]

A model of the single-engine nacelle, which was a 0.875-scale model of that used on the basic configuration, was also tested. This isolated nacelle was stabilized by three wedge-type fins swept back 45° along the leading edge and having a thickness of 3 percent chord.

## TESTS AND MEASUREMENTS

The rocket-propelled zero-lift models were tested at the Langley Pilotless Aircraft Research Station at Wallops Island, Va. Each model was propelled by a two-stage rocket system (as described in ref. 1) and launched from a rail launcher. Velocity and trajectory data were obtained from the CW Doppler velocimeter and the NACA modified SCR584 tracking radar unit, respectively. A survey of atmospheric conditions for each test was made through radiosonde measurements from an ascending balloon.

The flight tests covered a continuous range of Mach number $M$ varying from 0.8 to 1.3. The corresponding range of Reynolds number $R$ was from $4 \times 10^6$ to $7 \times 10^6$ based on wing mean aerodynamic chord as shown in figure 5.

The values of total drag coefficient $C_D$, based on total wing planform area, were calculated as in reference 1. The values of nacelle-plus-interference drag coefficient $C_{D_N}$ (based on the total frontal area of each nacelle tested) were obtained from the difference in drag coefficients of models with nacelles and a model without nacelles.

The isolated single-engine nacelle was tested by a flight-test technique suitable for small models. By this technique, the model was propelled to supersonic speeds by a compressed helium gun and then tracked with the same instrumentation used for the rocket-propelled models. The isolated nacelle test covered a Mach number range from 0.8 to 1.3 and a Reynolds number range (based on the wing mean aerodynamic chord of the basic wing-body configuration) from $4 \times 10^6$ to $6.5 \times 10^6$.

The magnitude of the error in drag coefficient was established from the test results of three identical models without nacelles in reference 1 and was based on the maximum deviation found between curves faired through the experimental points. At Mach numbers greater than 1.02, the repeatability of the measurements of total drag coefficient, nacelle-plus-interference drag coefficient, and Mach number are believed to be within the following limits:

[redacted]

| | |
|---|---|
| $C_D$ | ±0.0004 |
| $C_{D_N}$ | ±0.05 |
| M | ±0.005 |

The measurement of the drag coefficients and Mach number at high subsonic speeds and near Mach number 1.0 are less accurate than in the foregoing table and are believed to be within the following limits:

| | |
|---|---|
| $C_D$ | ±0.001 |
| $C_{D_N}$ | ±0.1 |
| M | ±0.005 |

## RESULTS AND DISCUSSION

Faired curves showing the variations of total drag coefficient with Mach number for the models tested herein and for two models, one with single-engine nacelles located inboard on the wing and one with single-engine nacelles at the wing tips, from reference 2 are presented in figure 6(a). The curve for the configuration without nacelles (model G) was obtained from reference 1. A comparison of the variations of $C_D$ with M in figure 6(a) shows that increasing the nacelle size or the number of nacelles on the wing panel resulted in an increase in the total drag coefficient throughout the Mach number range. It is evident in figure 6(a) that, for the large or multiengine nacelle arrangements, the lowest drag increment is obtained from the large tip nacelle (model C) near Mach number 1.0 and from the combination of single-engine nacelles (model D) at the inboard and wing-tip positions at Mach numbers greater than 1.05.

In recent investigations (refs. 7 to 10), a transonic drag-rise rule has been used to compare the drag rise of several wing-body configurations and to redesign the configurations to eliminate or greatly reduce the drag rise near Mach number 1.0. The successful application of the drag-rise rule, which simply states that the zero-lift drag rise for thin, low-aspect-ratio wing-body combinations near the speed of sound is primarily dependent on the axial distribution of the cross-sectional areas of the configuration normal to the axis of symmetry, has generated interest in its application to aircraft having high-aspect-ratio wings with external stores or nacelles. In this paper, therefore, the axial distribution of cross-sectional areas for the configurations tested and for two models from reference 2 are presented in figure 3 for comparison with the drag rises of the corresponding models shown in figure 6(a). It should be noted, however, that the configurations tested do not entirely meet the requirements of the drag-rise rule in that the wing is not thin and the aspect ratio is high, but partial fulfillment of the rule may be realized.

[redacted]

In order to compare the area diagrams (fig. 3) with the drag rises of the models, the cross-sectional area diagrams are assumed to represent bodies of revolution transformed from the various wing-body-nacelle combinations tested. Between Mach numbers of 0.8 and 1.0 in figure 6(a), it is evident that the models having the smallest drag rise are also the models that have the least rapid rate of development of cross-sectional areas and the smallest maximum cross-sectional areas as is shown in figure 3. A clear example of this observation may be found by comparing the area diagrams of models B and C, with the large nacelles mounted inboard and at the wing tips, respectively. By moving the large inboard nacelles (model B) to the wing tips (model C), to reduce the maximum cross-sectional area and the rate of development of the cross-sectional area, resulted in a large reduction in drag rise near Mach number 1.0. This same effect also is shown in figures 3 and 6(a) for models E and F with the single-engine nacelles at the inboard and wing-tip positions. In regard to the inboard positions of the twin-engine nacelle (model A) and the large nacelle (model B), both configurations have about the same maximum cross-sectional area, but model A has a more rapid rate of development of its cross-sectional area and, hence, a greater drag rise than model B. Although these models do not conform entirely to the requirements of the transonic drag-rise rule, it is apparent from these tests that the results are in general agreement with the concepts of the drag-rise rule.

The drag-rise Mach number of the basic configuration was reduced from 0.96 to approximately 0.90 when the large nacelle was mounted at the wing tip (model C) or located inboard on the wing (model B) and when the combination of single-engine nacelles (model D) at the wing tip and inboard positions were used. The model with the twin-engine nacelles (model A) reduced the drag-rise Mach number from 0.96 to about 0.88.

In order to compare the interference effects due to the nacelles and their locations, the variations of nacelle-plus-interference drag coefficient $C_{D_N}$ (based on the total frontal area of each nacelle) with Mach number for the models tested and for the two models from reference 2 are presented in figure 6(b) and are compared with the experimental drag coefficient of the single-engine isolated nacelle. In making a comparison of the nacelle-plus-interference drag coefficients in figure 6(b), it should be realized that there may be a significant shift in the level of some of the curves in figure 6(b) due to the relatively large error for $C_{D_N}$ with respect to the magnitude of $C_{D_N}$ over the Mach number range. However, values of $C_{D_N}$ less than the isolated nacelle drag coefficients in figure 6(b) generally indicate the presence of favorable interference effects.

[redacted]

The drag of the isolated single-engine nacelle was obtained by subtracting the drag of the three stabilizing fins from the experimental drag of the single-engine nacelle with the fins. The large nacelle, which had the same nose and afterbody shape as the single-engine nacelle, but a slightly smaller fineness ratio, is believed to have about the same drag coefficient as the single-engine nacelle over the flight range. The drag coefficient of the twin-engine nacelle may be greater than that of the axisymmetrical nacelles due to the two-dimensional wave drag over its flat upper and lower surfaces at transonic and supersonic Mach numbers.

From a comparison of the variations of $C_{D_N}$ with M in figure 6(b), it appears that favorable interference effects were obtained from all the nacelles between Mach numbers of 0.80 and 0.91, and, from the models with the single-engine nacelles (models D, E, and F) and with the large tip nacelles (model C) at Mach numbers above 1.0. The large unfavorable interference effects obtained at the inboard nacelle positions for the large nacelle (model B) and the twin-engine nacelle (model A) appear to result from a mutual interference effect between the nacelles and the fuselage. At the wing-tip position for the large nacelle (model C), where the nacelle is relatively far from the fuselage, less unfavorable interference effects were obtained near Mach number 1.0 than at the inboard position of the large nacelles. This reduction of unfavorable interference may be due to less unfavorable nacelle-fuselage interference at the wing tips than at the inboard positions and/or a favorable end-plate effect from the wing-tip nacelles. A similar effect of nacelle position on interference drag is shown also in figure 6(b) for the single-engine nacelles tested separately at the inboard and wing-tip positions. When the size of the single-engine nacelle was increased to that of the large or twin-engine nacelle, there was a large increase in interference drag, especially near Mach number 1.0, at corresponding nacelle positions. When the single-engine nacelles were combined at the inboard and wing-tip positions, no unfavorable interference effects were indicated over most of the Mach number range. It is evident from the foregoing comparisons that for an aircraft, similar to the basic configuration tested herein, requiring the thrust equivalency of four (persent-day) turbojet engines, use of two single-engine nacelles combined at the inboard and wing-tip positions on the wing panel or large single-engine nacelles at the wing tips would be most desirable from consideration of the drag.

## CONCLUSIONS

The effect on zero-lift drag of varying the size and number of symmetrically mounted nacelles on a 45° sweptback wing and body combination has been determined through flight tests of rocket-propelled

models between Mach numbers of 0.8 and 1.3. The configurations tested had the following nacelle arrangements on each wing panel: a twin-engine nacelle near the fuselage; a combination of single-engine nacelles, located at the wing tip and near the fuselage; a large nacelle at the wing tip; and a large nacelle near the fuselage. The following effects were noted:

1. The drag rises of the models were found to be in general agreement with the concepts of the transonic drag-rise rule.

2. For an aircraft similar to the basic configuration used herein, requiring the thrust equivalency of four (present-day) turbojet engines, use of two single-engine nacelles combined at the inboard and wing-tip positions on the wing panel or single-large-engine nacelles at the wing tips would be most desirable from a consideration of drag.

3. Increasing the size of the single-engine nacelles to that of the large nacelle or twin-engine nacelle resulted in an increase in nacelle-plus-interference drag coefficient, especially near Mach number 1.0.

4. The drag-rise Mach number of the basic configuration was reduced from 0.96 to about 0.90 by adding the large or single-engine nacelles to the wing and to about 0.88 by mounting the twin-engine nacelle near the fuselage.

Langley Aeronautical Laboratory
National Advisory Committee for Aeronautics
Langley Field, Va.

[redacted]

## REFERENCES

1. Pepper, William B., Jr., and Hoffman, Sherwood: Transonic Flight Tests to Compare the Zero-Lift Drag of Underslung and Symmetrical Nacelles Varied Chordwise at 40 Percent Semispan of a 45° Sweptback, Tapered Wing. NACA RM L50G17a, 1950.

2. Pepper, William B., Jr., and Hoffman, Sherwood: Comparison of Zero-Lift Drags Determined by Flight Tests at Transonic Speeds of Symmetrically Mounted Nacelles in Various Spanwise Positions on a 45° Sweptback Wing and Body Combination. NACA RM L51D06, 1951.

3. Hoffman, Sherwood: Comparison of Zero-Lift Drag Determined by Flight Tests at Transonic Speeds of Pylon, Underslung, and Symmetrically Mounted Nacelles at 40 Percent Semispan of a 45° Sweptback Wing and Body Combination. NACA RM L51D26, 1951.

4. Pepper, William B., Jr., and Hoffman, Sherwood: Comparison of Zero-Lift Drags Determined by Flight Tests at Transonic Speeds of Symmetrically Mounted Nacelles in Various Chordwise Positions at the Wing Tip of a 45° Sweptback Wing and Body Combination. NACA RM L51F13, 1951.

5. Hoffman, Sherwood: Transonic Flight Tests to Compare the Zero-Lift Drags of Underslung Nacelles Varied Spanwise on a 45° Sweptback Wing and Body Combination. NACA RM L52D04a, 1952.

6. Hoffman, Sherwood, and Pepper, William B., Jr.: Transonic Flight Tests to Determine Zero-Lift Drag and Pressure Recovery of Nacelles Located at the Wing Tips of a 45° Sweptback Wing and Body Combination. NACA RM L51K02, 1952.

7. Whitcomb, Richard T.: A Study of the Zero-Lift Drag-Rise Characteristics of Wing-Body Combinations Near the Speed of Sound. NACA RM L52H08, 1952.

8. Williams, Claude V.: A Transonic Wind-Tunnel Investigation of the Effects of Body Indentation, as Specified by the Transonic Drag-Rise Rule, on the Aerodynamic Characteristics and the Flow Phenomena of an Unswept-Wing—Body Combination. NACA RM L52L23, 1953.

9. Carmel, Melvin M.: Transonic Wind-Tunnel Investigation of the Effects of Aspect Ratio, Spanwise Variations in Section Thickness Ratio, and a Body Indentation on the Aerodynamic Characteristics of a 45° Sweptback Wing-Body Combination. NACA RM L52L26b, 1953.

[redacted]

10. Robinson, Harold R.: A Transonic Wind-Tunnel Investigation of the Effects of Body Indentation, as Specified by the Transonic Drag-Rise Rule, on the Aerodynamic Characteristics and Flow Phenomena of a 45° Sweptback-Wing—Body Combination. NACA RM L52L12, 1953.

[redacted]

TABLE I.- FUSELAGE COORDINATES

[Stations measured from fuselage nose]

| Station, in. | Ordinate, in. |
|---|---|
| 0 | 0 |
| .4 | .185 |
| .6 | .238 |
| 1.0 | .342 |
| 2.0 | .578 |
| 4.0 | .964 |
| 6.0 | 1.290 |
| 8.0 | 1.577 |
| 12.0 | 2.074 |
| 16.0 | 2.472 |
| 20.0 | 2.772 |
| 24.0 | 2.993 |
| 28.0 | 3.146 |
| 32.0 | 3.250 |
| 36.0 | 3.314 |
| 40.0 | 3.334 |
| 44.0 | 3.304 |
| 48.0 | 3.219 |
| 52.0 | 3.037 |
| 56.0 | 2.849 |
| 60.0 | 2.661 |
| 64.0 | 2.474 |
| 66.7 | 2.347 |

TABLE II.- COORDINATES OF THE NACA 65A009 AIRFOIL

| Station, percent chord | Ordinate, percent chord |
|---|---|
| 0 | 0 |
| .5 | .690 |
| .75 | .837 |
| 1.25 | 1.068 |
| 2.5 | 1.463 |
| 5.0 | 1.965 |
| 7.5 | 2.385 |
| 10.0 | 2.736 |
| 15.0 | 3.292 |
| 20.0 | 3.714 |
| 25.0 | 4.034 |
| 30.0 | 4.266 |
| 35.0 | 4.420 |
| 40.0 | 4.495 |
| 45.0 | 4.485 |
| 50.0 | 4.379 |
| 55.0 | 4.173 |
| 60.0 | 3.881 |
| 65.0 | 3.519 |
| 70.0 | 3.099 |
| 75.0 | 2.630 |
| 80.0 | 2.125 |
| 85.0 | 1.601 |
| 90.0 | 1.074 |
| 95.0 | .547 |
| 100.0 | .020 |
| L.E. radius = 0.516 percent chord | |

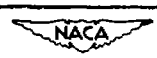


[redacted]

TABLE III.- COORDINATES FOR SINGLE-ENGINE NACELLE[1]

[Station measured from nacelle nose]

| Station, in. | Ordinate, in. |
|---|---|
| 0 | 0 |
| .100 | .070 |
| .330 | .169 |
| .830 | .336 |
| 1.330 | .489 |
| 1.830 | .622 |
| 2.330 | .747 |
| 2.580 | .800 |
| 2.958 | .876 |
| 3.585 | .974 |
| 4.840 | 1.105 |
| 6.095 | 1.190 |
| 7.350 | 1.240 |
| 8.605 | 1.255 |
| 16.830 | 1.255 |
| 17.872 | 1.237 |
| 18.913 | 1.195 |
| 19.955 | 1.127 |
| 20.996 | 1.029 |
| 22.038 | .909 |
| 23.079 | .768 |
| 24.121 | .616 |
| 24.250 | .598 |
| Nose radius = 0.05 in. | |

[1]The twin-engine nacelle consists of two single-engine nacelles tangent at the cylindrical sections in the wing plane and faired with straight line elements at the upper and lower surfaces.

TABLE IV.- COORDINATES FOR LARGE NACELLE

[Station measured from nacelle nose]

| Station, in. | Ordinate, in. |
|---|---|
| 0.000 | 0.000 |
| .150 | .105 |
| .495 | .254 |
| 1.245 | .504 |
| 1.995 | .734 |
| 2.745 | .933 |
| 3.495 | 1.121 |
| 4.437 | 1.314 |
| 5.378 | 1.461 |
| 6.789 | 1.616 |
| 8.202 | 1.728 |
| 10.085 | 1.829 |
| 12.908 | 1.883 |
| 21.133 | 1.883 |
| 22.969 | 1.856 |
| 24.258 | 1.793 |
| 25.821 | 1.691 |
| 27.375 | 1.544 |
| 28.945 | 1.362 |
| 30.507 | 1.152 |
| 32.070 | .924 |
| 32.262 | .897 |
| Nose radius = 0.075 in. | |

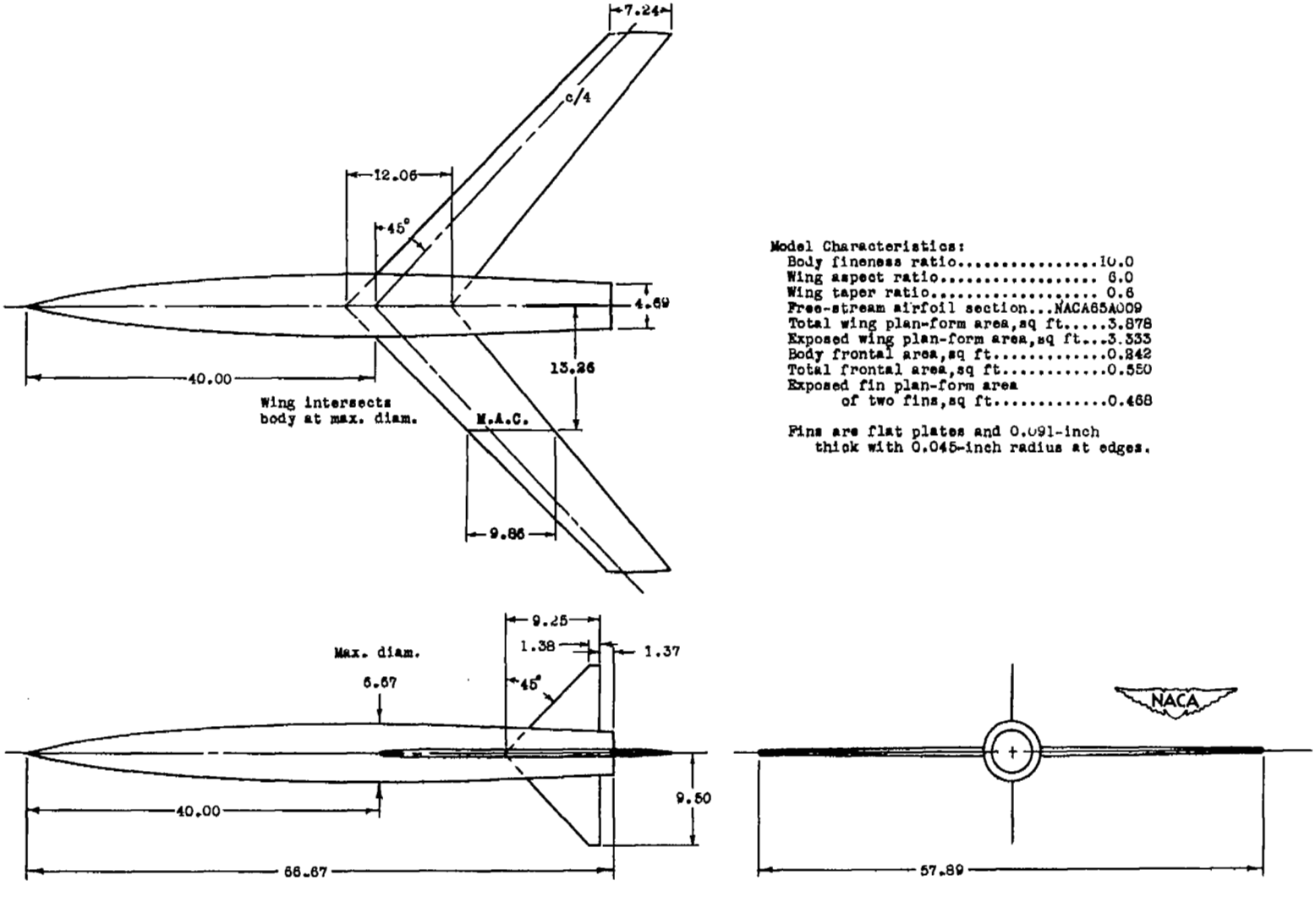


Model Characteristics:

| | |
|---|---|
| Body fineness ratio | 10.0 |
| Wing aspect ratio | 6.0 |
| Wing taper ratio | 0.6 |
| Free-stream airfoil section | NACA65A009 |
| Total wing plan-form area, sq ft | 3.878 |
| Exposed wing plan-form area, sq ft | 3.333 |
| Body frontal area, sq ft | 0.842 |
| Total frontal area, sq ft | 0.550 |
| Exposed fin plan-form area of two fins, sq ft | 0.468 |

Fins are flat plates and 0.091-inch thick with 0.045-inch radius at edges.

Figure 1.- General arrangement and dimensions of test model.
All dimensions are in inches.

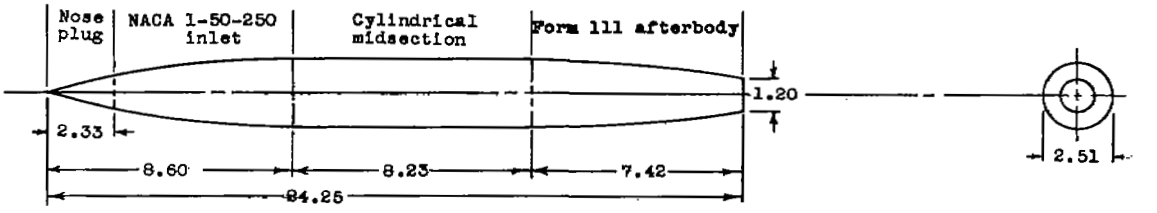


Nacelle frontal area = 0.034 sq. ft.
Nacelle fineness ratio = 9.66

(a) Single engine nacelle

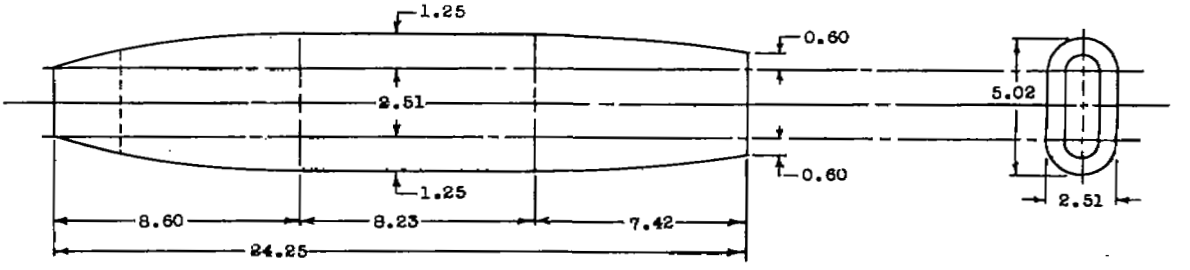


Nacelle frontal area = 0.078 sq. ft.

(b) Twin-engine nacelle

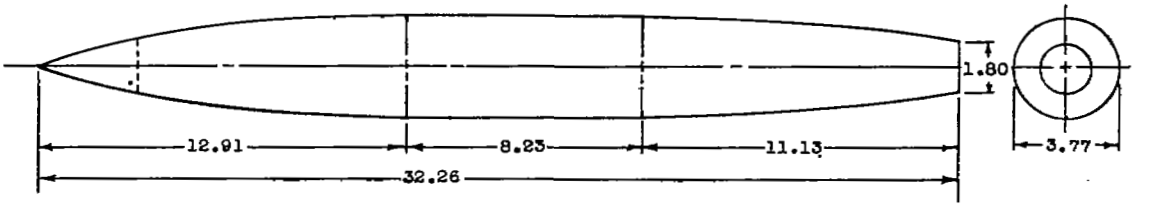


Nacelle frontal area = 0.077 sq. ft.
Nacelle fineness ratio = 8.56

(c) Large nacelle

NACA

Figure 2.- Details and dimensions of nacelles. All dimensions are in inches.

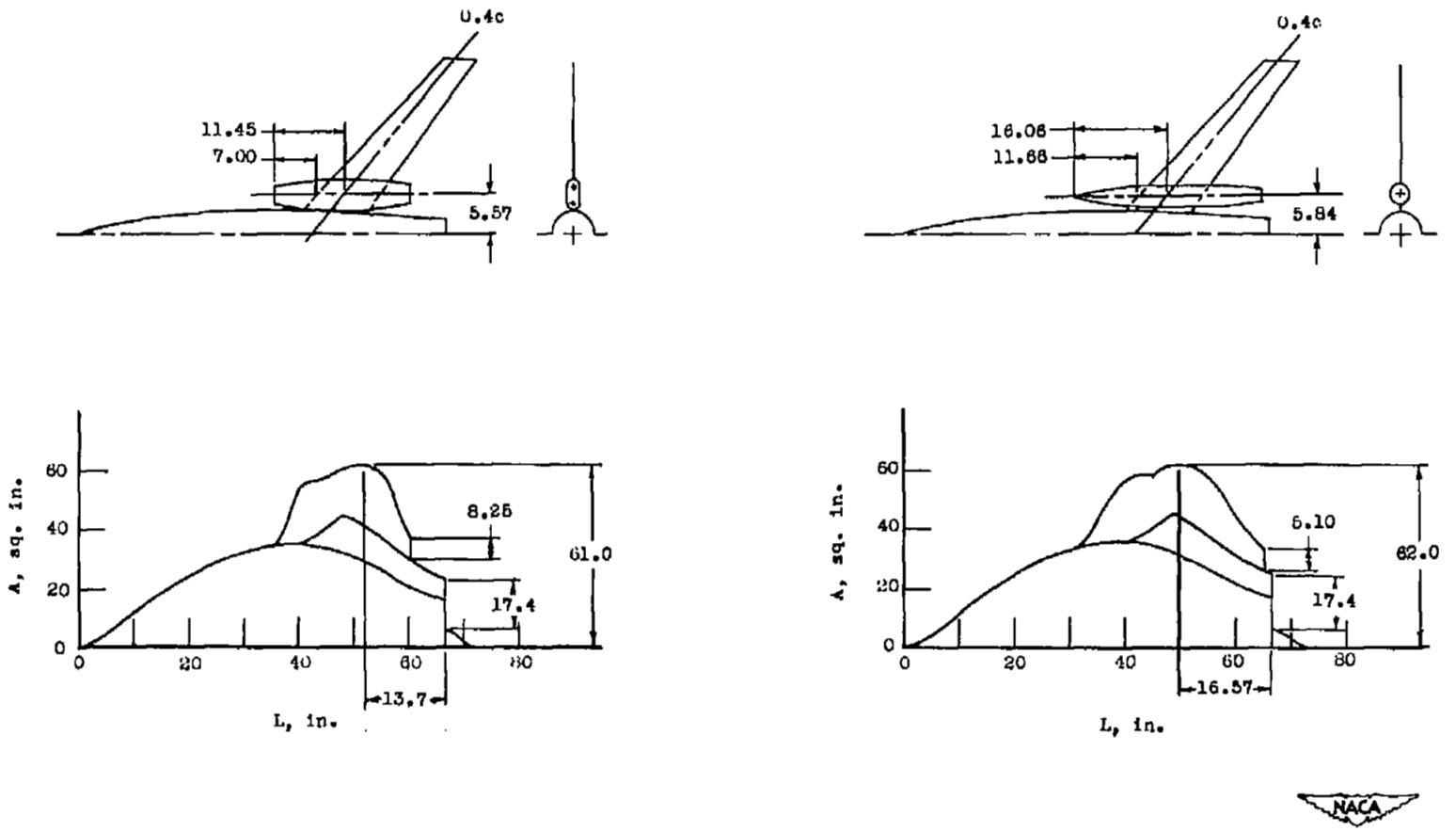


(a) Twin-engine nacelle near fuselage (model A).

(b) Large nacelle near fuselage (model B).

Figure 3.- Details of nacelle locations and cross-sectional area distributions of models. All dimensions are in inches.

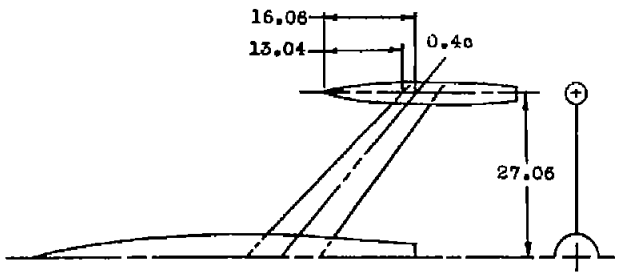


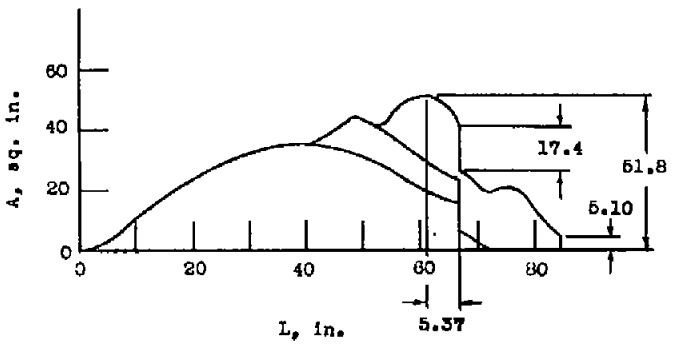


(c) Large nacelle near wing tip (model C).

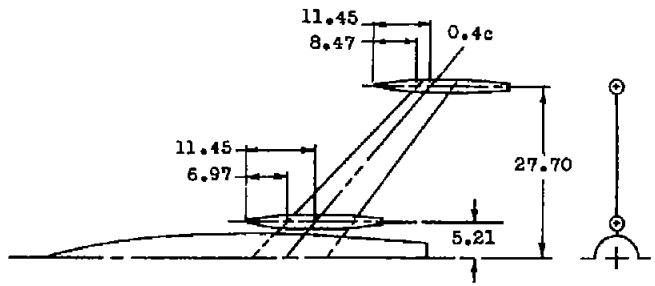


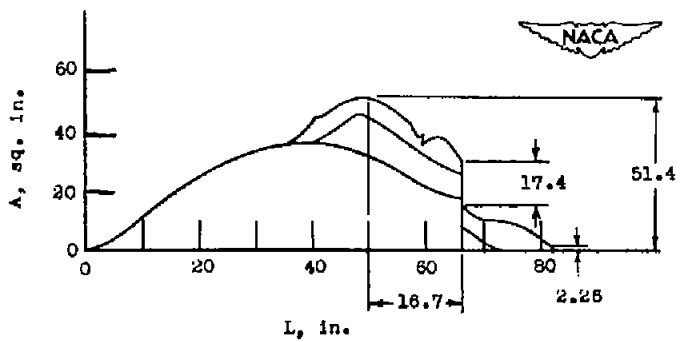


(d) Single engine nacelles near fuselage and at wing tip (model D).

Figure 3.- Continued.

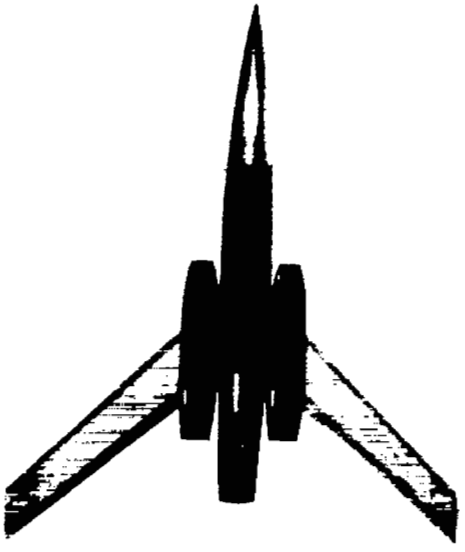

(a) Model A.

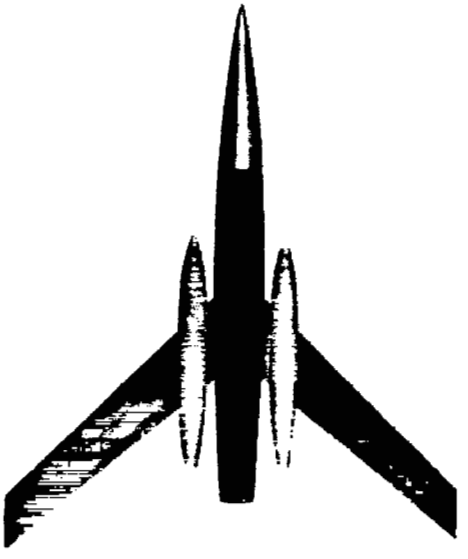

(b) Model B.

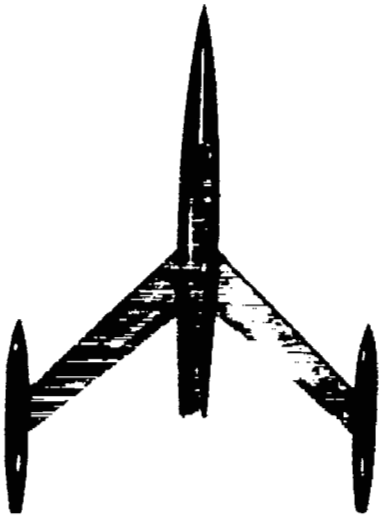

(c) Model C.

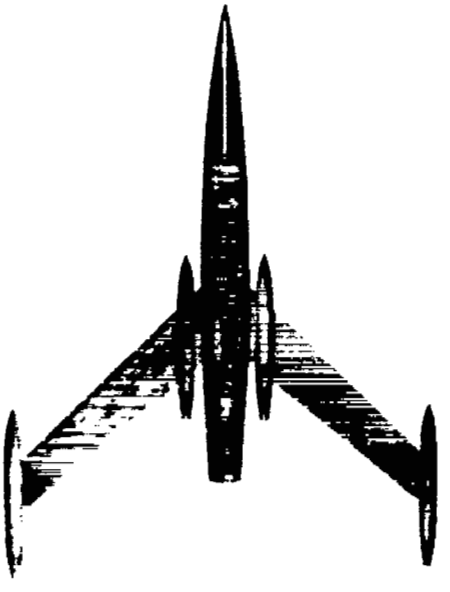

(d) Model D.

NACA L-79264

Figure 4.- Photographs showing test models.

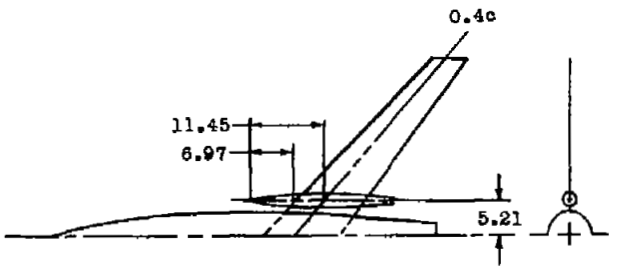


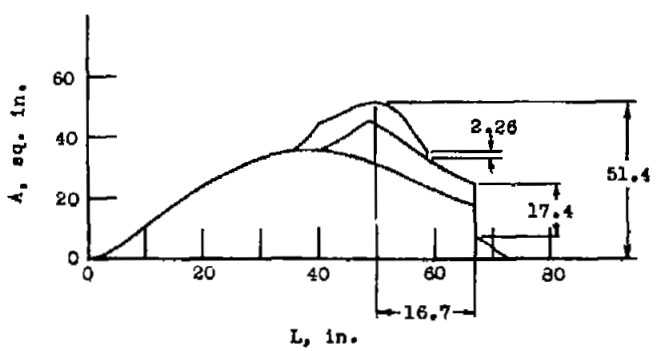


(e) Single engine nacelle near fuselage (ref. 2).

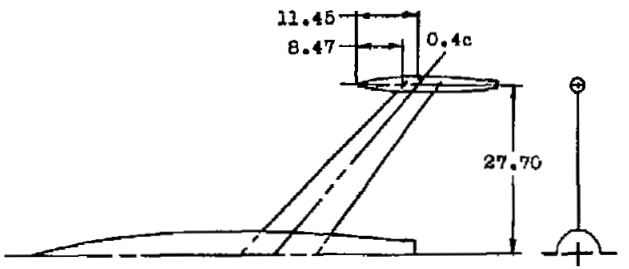


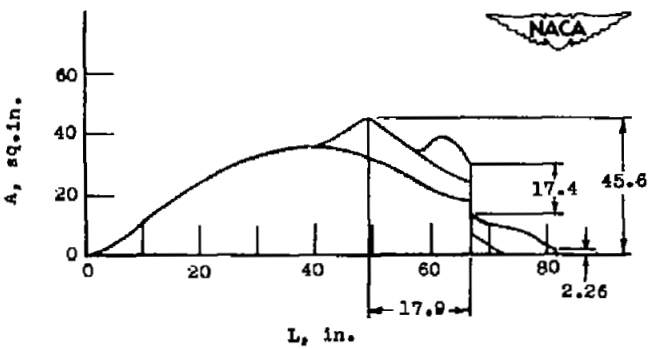


(f) Single engine nacelle at wing tip (ref. 2).

Figure 3.- Concluded.

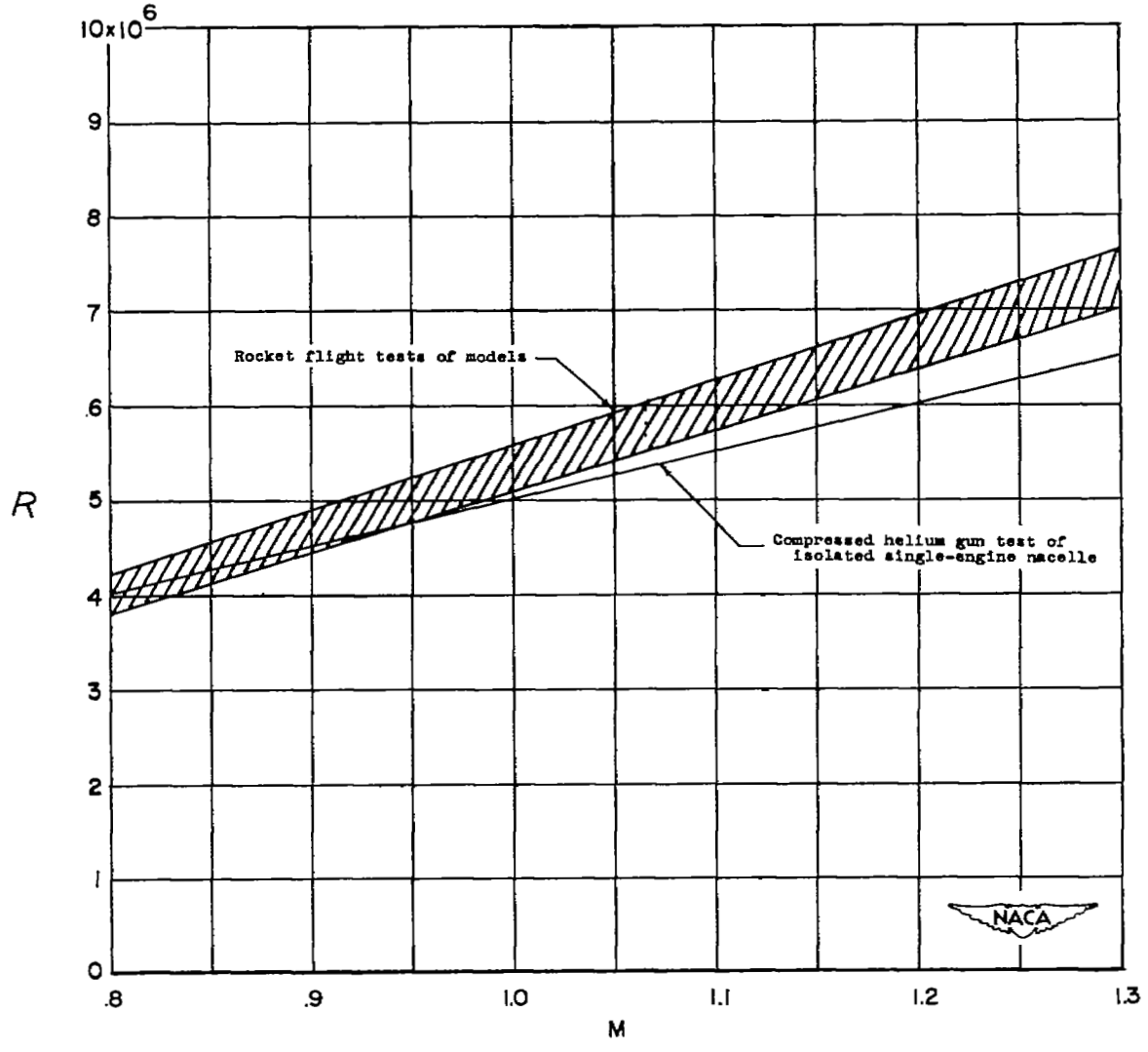


Figure 5.- Variation of Reynolds number with Mach number for models tested. Reynolds number based on wing mean aerodynamic chord.

[redacted]

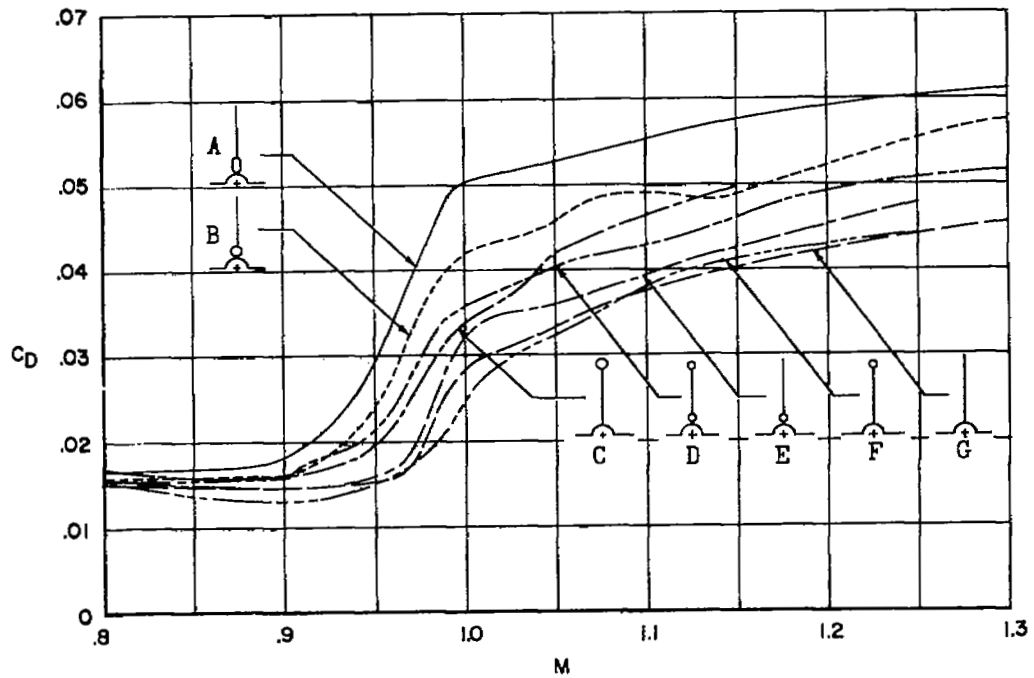


(a) Variations of total drag coefficients with Mach number.

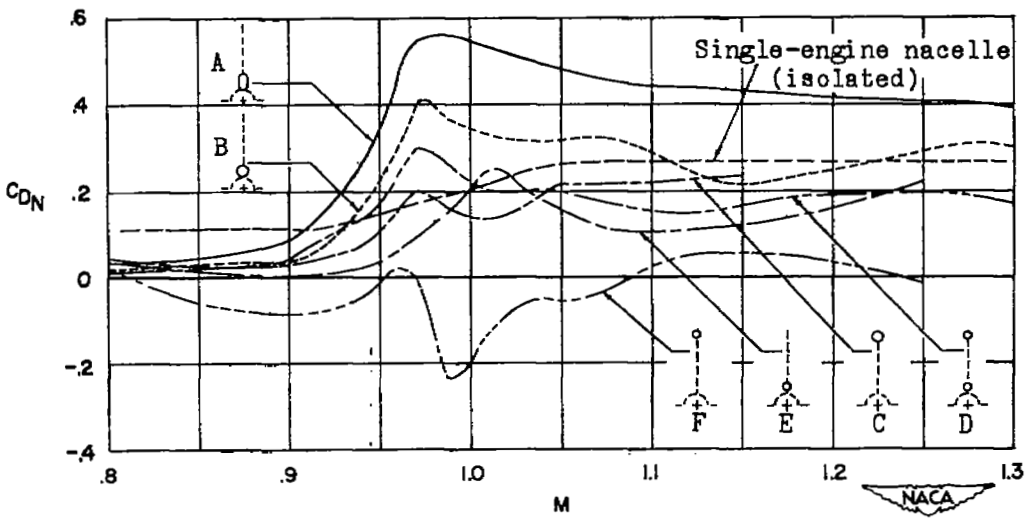


(b) Variations of nacelle-plus-interference drag coefficients with Mach number.

Figure 6.- Variations of total drag coefficients and nacelle-plus-interference drag coefficients with Mach number for models tested: Data for models E and F from reference 2 and for model G from reference 1.

[redacted]



[redacted]